Hindawi
Journal of Nanomaterials
Volume 2020, Article ID 1584310, 11 pages
https://doi.org/10.1155/2020/1584310

Research Article

Magnetic Properties, Adhesion, and Nanomechanical Property of $Co_{40}Fe_{40}W_{20}$ Films on Si (100) Substrate

Wen-Jen Liu,[1] Yung-Huang Chang,[2] Sin-Liang Ou,[3] Yuan-Tsung Chen,[4] You-Cheng Liang,[4] Bo-Jia Huang,[4] Chun-Lin Chu,[5] Chia-Chin Chiang,[6] and Te-Ho Wu[4]

[1]*Department of Materials Science and Engineering, I-Shou University, Kaohsiung 840, Taiwan*
[2]*Bachelor Program in Interdisciplinary Studies, National Yunlin University of Science and Technology, 123 University Road, Section 3, Douliou, Yunlin 64002, Taiwan*
[3]*Bachelor Program for Design and Materials for Medical Equipment and Devices, Da-Yeh University, Changhua 51591, Taiwan*
[4]*Graduate School of Materials Science, National Yunlin University of Science and Technology, 123 University Road, Section 3, Douliou, Yunlin 64002, Taiwan*
[5]*National Applied Research Laboratories, Taiwan Semiconductor Research Institute, Hsinchu, Taiwan 30078*
[6]*Department of Mechanical Engineering, National Kaohsiung University of Science and Technology, No. 415, Jiangong Rd., Sanmin District, Kaohsiung City 807, Taiwan*

Correspondence should be addressed to Yuan-Tsung Chen; ytchen@yuntech.edu.tw

Received 21 February 2020; Revised 7 May 2020; Accepted 19 May 2020; Published 20 July 2020

Academic Editor: Ping Xiao

Copyright © 2020 Wen-Jen Liu et al. This is an open access article distributed under the Creative Commons Attribution License, which permits unrestricted use, distribution, and reproduction in any medium, provided the original work is properly cited.

In this study, a $Co_{40}Fe_{40}W_{20}$ alloy was sputtered onto Si (100) with thicknesses (t_f) ranging from 18 to 90 nm, and the corresponding structure, magnetic properties, adhesive characteristics, and nanomechanical properties were investigated. X-ray diffraction (XRD) patterns of the $Co_{40}Fe_{40}W_{20}$ films demonstrated a significant crystalline body-centered cubic (BCC) CoFe (110) structure when the thickness was 42 nm, and an amorphous status was shown when the thickness was 18 nm, 30 nm, 60 nm, and 90 nm. The saturation magnetization (M_s) showed a saturated trend as t_f was increased. Moreover, the coercivity (H_c) showed a minimum 1.65 Oe with 30 nm. H_c was smaller than 4.5 Oe owing to the small grain size distribution and amorphous structure, indicating that the $Co_{40}Fe_{40}W_{20}$ film had soft magnetism. The low-frequency alternating current magnetic susceptibility (χ_{ac}) decreased as the frequency was increased. The χ_{ac} revealed a thickness effect when greater thicknesses had a large χ_{ac}. The maximum χ_{ac} and optimal resonance frequency (f_{res}) of $Co_{40}Fe_{40}W_{20}$ were investigated. The maximum χ_{ac} indicated the spin sensitivity and was maximized at the optimal resonance frequency. The 90 mm thickness had the highest χ_{ac} 0.18 value at an f_{res} of 50 Hz. The contact angles of the $Co_{40}Fe_{40}W_{20}$ films are less than 90°, which indicated that the film had a good wetting effect and hydrophilicity. The surface energy was correlated with the adhesion and displayed a concave-down trend. CoFeW films can be used as a seed or buffer layer; therefore, the surface energy and adhesion are very important. The highest surface energy was 30.12 mJ/mm^2 at 42 nm and demonstrated high adhesion. High surface energy has corresponding strong adhesive performance. The increased surface roughness can induce domain wall pinning effect and high surface energy, causing a high coercivity and strong adhesion. The increase of hardness and Young's modulus could be reasonably inferred from the thinner CoFeW films. The hardness and Young's modulus of CoFeW films are also displayed to saturated tendency when increasing thickness.

1. Introduction

In recent years, the direction of information storage is gradually developing to the field of magnetic recording, in which CoFe is one of the most studied alloys. In 2002, George et al. added 2% vanadium (V) to CoFe alloy and improved its brittleness to promote low-temperature application [1]. The CoFe layer can be a pinned layer or a free layer in the spin-valued magnetic tunneling junction (MTJ), which can be applied to the magnetoresistance random access memory

(MRAM) and recording head applications [2–7]. Adding B and V elements to CoFe data has advantages in my previous work, including mechanical strength and magnetic properties [8]. At present, tungsten (W) is added to CoFe data to study its mechanical strength and magnetic properties. W is a hard metal with high melting temperature. In recent years, researchers have increased attention to adding a novel third element into the original CoFe matrix in magnetic fields [9–14]. However, few studies have focused on adding W to CoFe. In 2012, Pai et al. investigated the thickness phase transition of rare earth transition metal W [15]. In this reference, W is used as a seed layer to study the effect of MTJ spin Hall angle. In 2016, Ghaferi et al. studied the composition ratio of tungsten in CoFeW alloy with citrate borate solution, and the morphology, microstructure, and magnetic properties of these films at different pH values were analyzed [16]. The results show that the CoFeW alloy has low coercivity (H_c) due to the grain refinement. Sun et al. also provided an important discussion on CoFeW ternaries based on oxygen evolution reactions [17]. Compared with other materials, CoFe alloy has high saturation magnetization (M_s) [18–21]. However, adding W as the third element can improve the mechanical properties of CoFe alloy [22]. In addition, a CoFeW layer can be combined with the magnetic process and be compatible with other layers in bilayered or multilayered systems. The adhesion of CoFeW film is an important characteristic of its compatibility with other films. For these reasons, it is of great significance to study the magnetic properties, adhesion, and nanomechanical properties of CoFeW films by sputtering deposition technology.

2. Experimental Details

CoFeW was deposited onto a Si (100) substrate at room temperature (RT) in thicknesses (t_f) ranging from 18 to 90 nm using the direct current (DC) method at a power of 50 W. Moreover, the power density was 1.65 W/cm^2, and the deposition rate was 1.2 nm/min. The geometry of the deposition system is square, and the target-substrate distance is approximately 15 cm. The target composition of the CoFeW alloy was 40 at% Co, 40 at% Fe, and 20 at% W. The typical base chamber pressure was 2.6×10^{-7} Torr, and the Ar working chamber pressure was 3×10^{-3} Torr. The structure of $Co_{40}Fe_{40}W_{20}$ thin films was detected by X-ray diffraction (XRD) of $CuK_{\alpha 1}$ (Philips X'pert). In addition, the in-plane low-frequency alternate-current magnetic susceptibility (χ_{ac}) of $Co_{40}Fe_{40}W_{20}$ was studied using a χ_{ac} analyzer (XacQuan). Firstly, the χ_{ac} analyzer with external magnetic field is used to calibrate the reference standard sample. Then, insert the tested sample into the χ_{ac} analyzer. The driving frequency is between 10 and 25000 Hz. The χ_{ac} was determined by magnetization measurement. All tested samples have the same shape and size to eliminate demagnetization factors. The χ_{ac} valve is an arbitrary unit (a.u.), because the alternating current result corresponds to the reference standard sample and is a comparative value. The χ_{ac} analyzer measured the relationship between susceptibility and frequency. The optimal resonance frequency (f_{res}) is measured by the χ_{ac} analyzer, which represents the frequency of the maximum χ_{ac}. The in-plane hysteresis loop of the $Co_{40}Fe_{40}W_{20}$ films was obtained by an alternating gradient magnetometer (AGM). Finally, using deionized (DI) water and glycerol as experimental liquids, the surface energy of $Co_{40}Fe_{40}W_{20}$ thin films was calculated by measuring the contact angle [23–25]. It is defined as the surface excess-free energy of a specific crystal surface area [26]. To investigate the relation of coercivity (H_c) and surface energies, the surface roughness of CoFeW films was examined by atomic force microscopy (AFM). Hardness and Young's modulus of the CoFeW thin films were measured using an MTS Nano Indenter XP with a Berkovich indenter. An indentation load of 1 mN was used to limit the depth of penetration of the indenter to less than 10% of the film thickness. The indentation load was increased in 40 steps, and the penetration depth was measured at each step. Six indentations were investigated in each sample and averaged with a standard deviation for more accurate results.

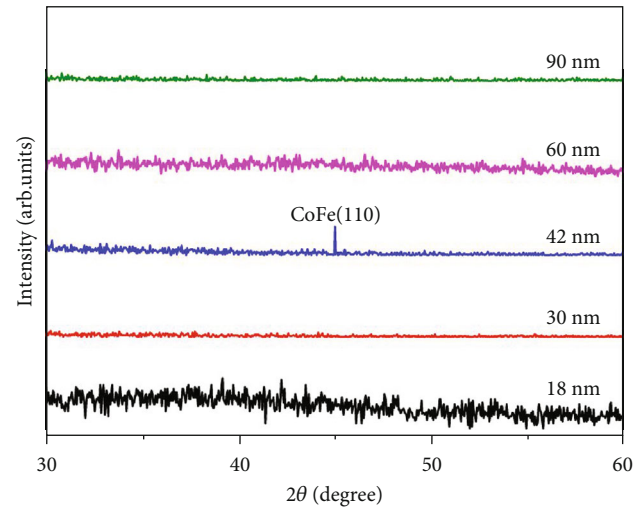

Figure 1: XRD results for $Co_{40}Fe_{40}W_{20}$ films.

3. Results and Discussion

3.1. Structure Property. Figure 1 shows the X-ray diffraction (XRD) of the $Co_{40}Fe_{40}W_{20}$ film. Because the intensity of the Si (100) peak on the single crystal substrate is stronger than that of the CoFeW crystallization, the XRD is presented at diffracted angle (2θ) between 30 and 60 degrees. An especially high crystalline body-centered cubic (BCC) CoFe (110) peak occurred at 42 nm because it can be reasonably concluded that it had a continuous mode of film growth and induced strong crystallization. The CoFeW films showed an amorphous status when the thicknesses at 18 nm, 30 nm, 60 nm, and 90 nm. It can also be reasonably concluded that the $Co_{40}Fe_{40}W_{20}$ thickness will have discontinuous growth model and random arrangement of atoms, leading to amorphous state [27]. The 42 nm of the CoFeW thin film has a strong crystallization, while the other thicker and thinner films are amorphous. It can be reasonable that this sputtering

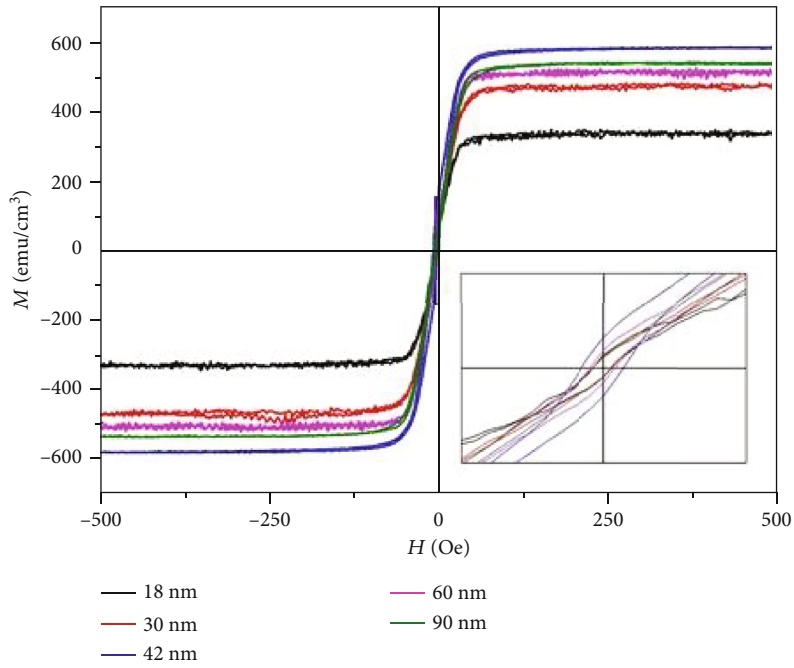

Figure 2: In-plane magnetic hysteresis loop of $Co_{40}Fe_{40}W_{20}$ thin films.

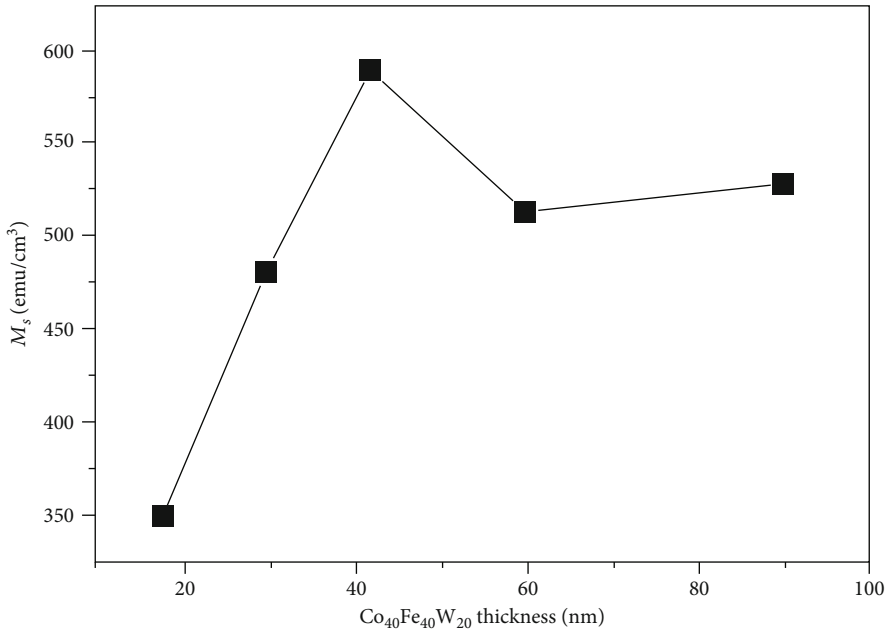

Figure 3: Saturation magnetization (M_s) of $Co_{40}Fe_{40}W_{20}$ thin films.

condition of 42 nm may be slightly different from other films and induces this result [28].

3.2. Magnetic Properties. Figure 2 depicts the hysteresis loop of the $Co_{40}Fe_{40}W_{20}$ film using AGM measurement. The in-plane magnetic field (H_{ext}) of 500 Oe is enough to detect the saturated magnetic spin state. The results also show that the $Co_{40}Fe_{40}W_{20}$ film has low coercivity (H_c) and soft magnetic properties.

The saturation magnetization (M_s) of the $Co_{40}Fe_{40}W_{20}$ film is shown in Figure 3. The results show that there is a significant relationship between M_s and thickness. When the film thickness increases from 18 nm to 90 nm, M_s shows a saturated trend, which shows the thickness effect of M_s in the $Co_{40}Fe_{40}W_{20}$ film. The maximum M_s at 42 nm is about 590 emu/cm^3 owing to strong magneto-crystalline anisotropy, which indicates that it has high spin coupling strength and can induce large M_s.

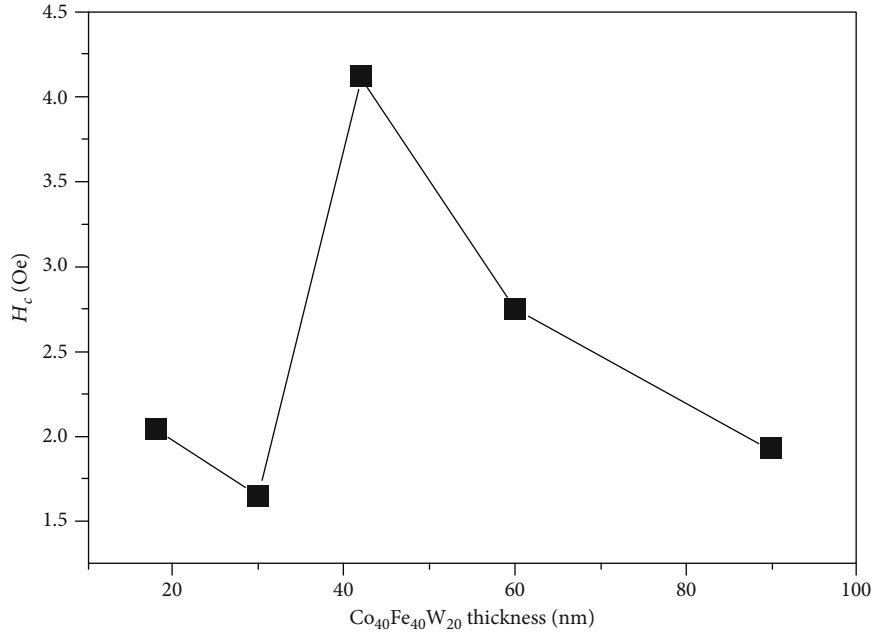

Figure 4: Coercivity (H_c) of $Co_{40}Fe_{40}W_{20}$ thin films.

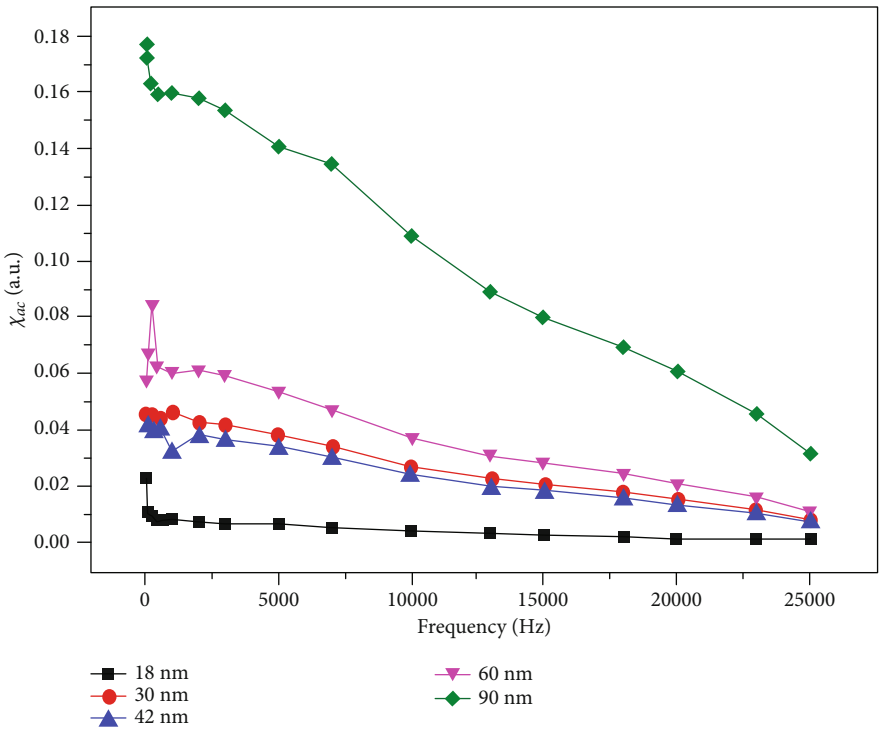

Figure 5: The low-frequency alternate-current magnetic susceptibility (χ_{ac}) as a function of the frequency from 10 to 25,000 Hz.

The corresponding H_c is shown in Figure 4. When t_f is in the range from 18 to 30 nm, H_c decreases from 2.04 Oe to 1.65 Oe. When t_f is in the range from 30 to 42 nm, H_c increases from 1.65 Oe to 4.12 Oe. Finally, H_c decreased to 1.93 Oe at 90 nm. The maximum H_c was 4.12 Oe at 42 nm due to the pinning effect of the domain wall, which was not easy to move, resulting in the increase in coercivity [29, 30]. The amorphous structure of the $Co_{40}Fe_{40}W_{20}$ films indicated a smaller H_c due to the small grain size distribution [31, 32]. A strong crystalline peak occurred at 42 nm in XRD result.

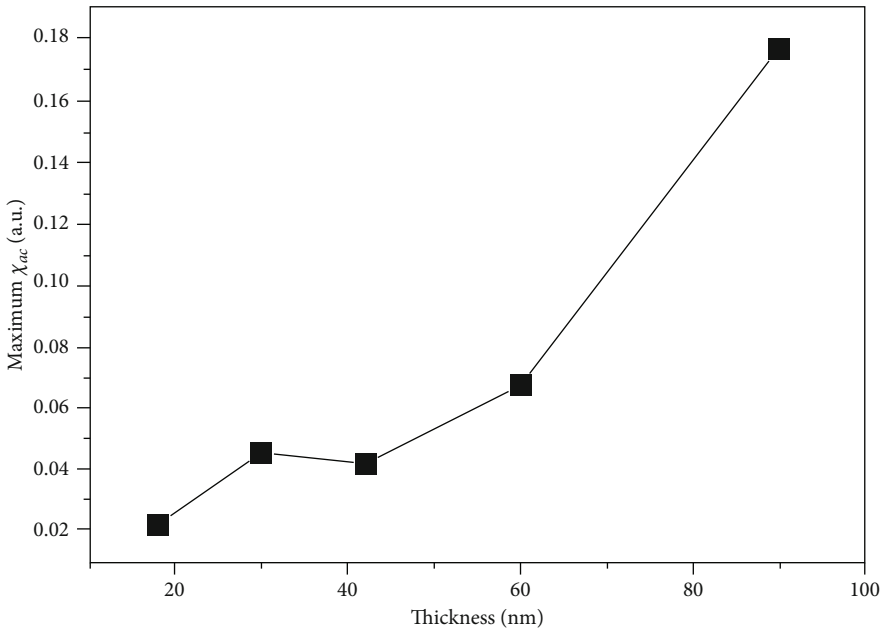

Figure 6: Maximum alternate-current magnetic susceptibility for the CoFeW films.

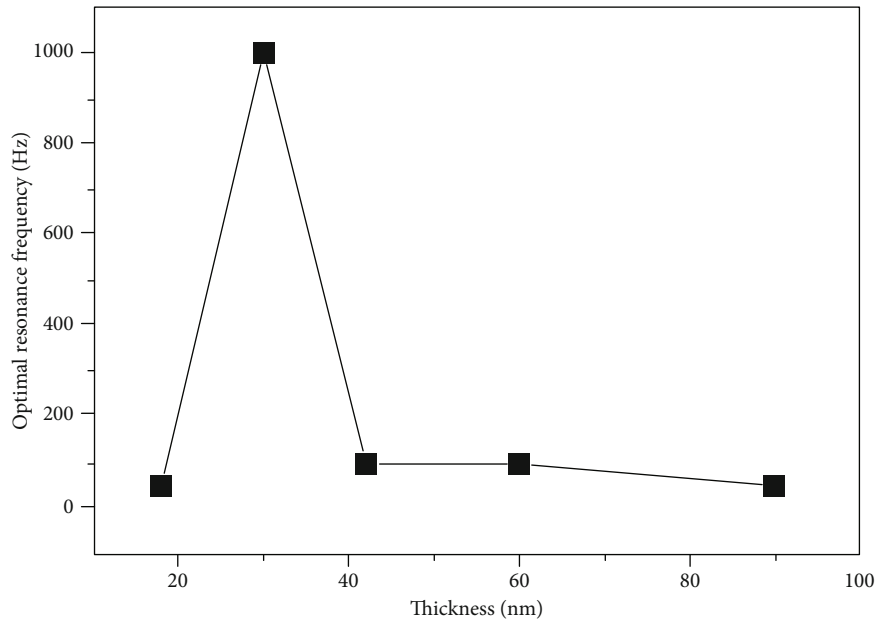

Figure 7: Optimal resonance frequency for films of various thicknesses.

According to Scherrer's formula (1), the average grain size (D) can be estimated from the full width measured at the half-height width (FWHM, B) of the 42 nm diffraction peak. Scherrer's formula is [33]

$$D = \frac{k\lambda}{B\cos\theta}. \quad (1)$$

In the formula, k (0.89) is the Scherrer's constant, λ is the X-ray wavelength of the $CuK_{\alpha 1}$ line, B is the FWHM of the 42 nm diffraction peak, and θ is the half angle of the diffraction peak. This formula shows that D is proportional to $1/B$, so smaller B corresponds to larger grains. The 42 nm of $Co_{40}Fe_{40}W_{20}$ thin film has a smaller B and can induce larger grains to be deposited. Furthermore, the large grain size distribution has higher H_c [34, 35].

The H_c value is lower than 4.5 Oe, which indicates that the $Co_{40}Fe_{40}W_{20}$ film has soft magnetic properties and is suitable for MRAM and magnetic head applications.

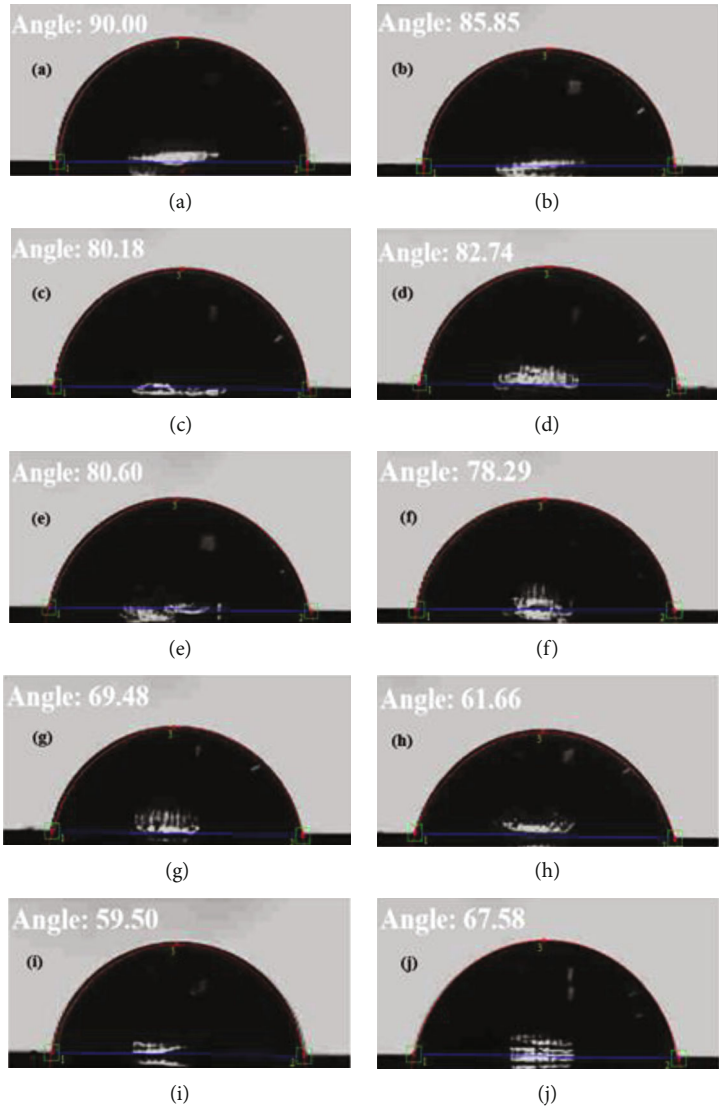

FIGURE 8: Contact angles of the $Co_{40}Fe_{40}W_{20}$ thin films with DI water: (a) 18 nm, (b) 30 nm, (c) 42 nm, (d) 60 nm, and (e) 90 nm. Contact angles of the $Co_{40}Fe_{40}W_{20}$ thin films with glycerol: (f) 18 nm, (g) 30 nm, (h) 42 nm, (i) 60 nm, and (j) 90 nm.

Figure 5 shows the χ_{ac} results of the CoFeW film. The results show that the χ_{ac} value increases with the increase of t_f in the range of 18 nm to 90 nm. With the increase of measurement frequency, χ_{ac} decreases sharply.

The maximum χ_{ac} corresponding to different thickness of CoFeW is shown in Figure 6. Due to the thickness effect, when t_f increases from 18 nm to 90 nm, the maximum χ_{ac} increases from 0.02 to 0.18. The results show that the spin sensitivity is the strongest at the optimal resonance frequency (f_{res}). The maximum χ_{ac} at the optimal resonance frequency has the following physical significance. At low frequency, the alternating-current dipole moment is caused by the volume dipole moment oscillation in each domain. The external alternating-current magnetic field plays a driving role. The recovery of the magnetic interaction occurred between domains. A resonance frequency acted as the driving force acting on the system. Therefore, the peak frequency of the low frequency susceptibility corresponds to the resonance frequency of the pole moment oscillation. In frequency, χ_{ac} peak represents spin exchange coupling interaction and domain dipole moment [8, 36].

The optimal resonance frequency (f_{res}) of CoFeW film is shown in Figure 7. At this frequency, the maximum χ_{ac} is measured with the strongest spin sensitivity [36, 37]. The f_{res} shows a downward concave trend with a maximum critical frequency of 1000 Hz. The f_{res} values of all CoFeW thicknesses are less than 1000 Hz, indicating that the film is advantageous to the application of sensors, transformers, and low-frequency magnetic recording media.

3.3. Analysis of Surface Energy and Adhesion. Figure 8 illustrates the contact angle of CoFeW films using deionized (DI) water and glycerin. The results show that the water droplets on the CoFeW film are nearly spherical and the

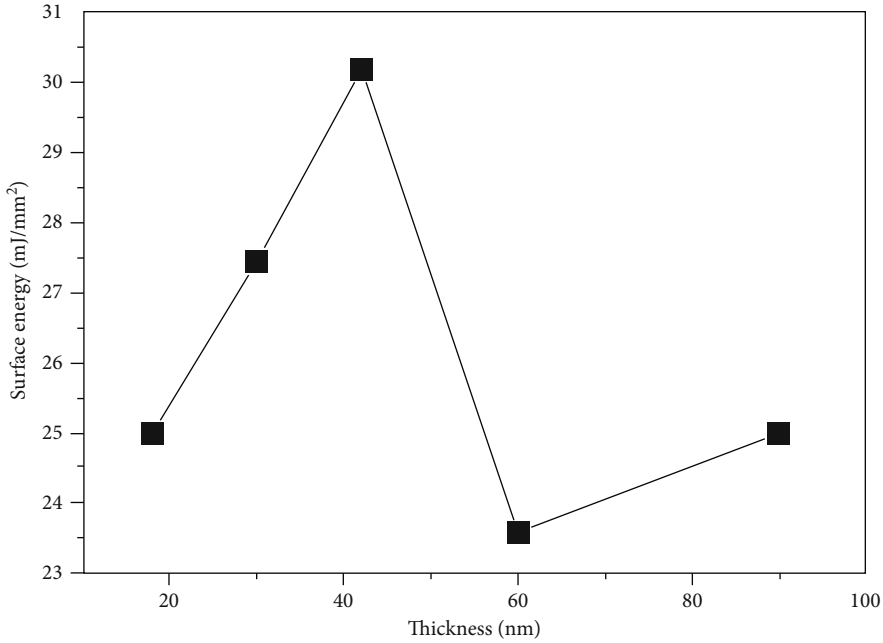

FIGURE 9: Surface energy of $Co_{40}Fe_{40}W_{20}$ thin films.

contact angle is less than 90°, indicating that the film has good wettability and hydrophilicity. The CoFeW film can be used as a seed layer or a buffer layer, and its surface energy and adhesion are very important. When the surface energy is high, the liquid absorption is large and the liquid absorption area is large, resulting in the decrease of the contact angle [8, 38].

Figure 9 shows the calculated surface energy using the contact angle [23–25]. Due to the larger pinning effect of domain walls, the surface energy results show a downward concave trend, and the maximum critical value at 42 nm is 30.12 mJ/mm^2 [28, 29]. Low surface energy corresponds to weak adhesion [39]. Therefore, the adhesion of 42 nm film is higher than that of other $Co_{40}Fe_{40}W_{20}$ films.

3.4. Analysis of Surface Roughness. To confirm the relation of coercivity and surface energies, the surface roughness of CoFeW films was detected by AFM, which is shown in Figures 10(a)–10(e). When the thickness is increased from 18 nm to 90 nm, the root mean square values (R_q) of surface roughness are 0.41 nm, 0.35 nm, 0.63 nm, 0.59 nm, and 0.47 nm, respectively. The increased surface roughness can lead to the pinning effect of the domain wall, which is not easy to move, resulting in the increase in coercivity [40, 41]. Moreover, the rough surface roughness can be induced high surface energy, causing a high adhesion [42, 43]. This result is consistent with Figures 4 and 9.

3.5. Analysis of Nanoindentation. Figures 11(a) and 11(b) show that the hardness and Young's modulus increase with the increase of the thickness of the CoFeW film. In general, nanoindentation hardness is determined from the loading unloading curve by the Pharr-Oliver method [44], which indicates the mixed hardness of silicon substrate and CoFeW film. Because the thicknesses of CoFeW films are too thin, it can be reasonably concluded that the substrate effect must exist in nanoindentation measurement. The corresponding hardness and Young's modulus values of the substrate are 4.12 GPa and 133.3 GPa in the nanoindentation measurement. To reduce the silicon substrate effect, the experimental results carried out for this work average value and standard deviation must be presented in the error bar in Figures 11(a) and 11(b). When the thickness increased from 18 nm to 90 nm, the hardness and Young's modulus of CoFeW films increased from 4.02 GPa to 10.94 GPa and 132.1 GPa to 186.3 GPa, respectively. The hardness and Young's modulus of CoFeW films are also displayed to saturated tendency when the thickness is from 18 nm to 90 nm. According to the result, the Young's modulus of adding the W effect to CoFe films in thicker films is larger than that of the CoFe film. The influence of thinner CoFeW films on the substrate is more significant, which is consistent with the phenomenon [45].

4. Conclusions

XRD patterns of the $Co_{40}Fe_{40}W_{20}$ films demonstrated a significant crystalline body-centered cubic (BCC) CoFe (110) structure when the thickness was 42 nm. The other films showed an amorphous status. The highest χ_{ac} value was 0.18 at 90 nm at an f_{res} value of 50 Hz. The f_{res} value was less than 1000 Hz at all thicknesses, demonstrating that the CoFeW films were suitable for magnetic component applications in low-frequency environments. The H_c indicated that the critical thickness was 42 nm due to a greater pinning site effect, which induced high H_c and strong adhesion. The H_c value was smaller than 4.5 Oe, owing to small a grain size distribution and amorphous structure and indicating that

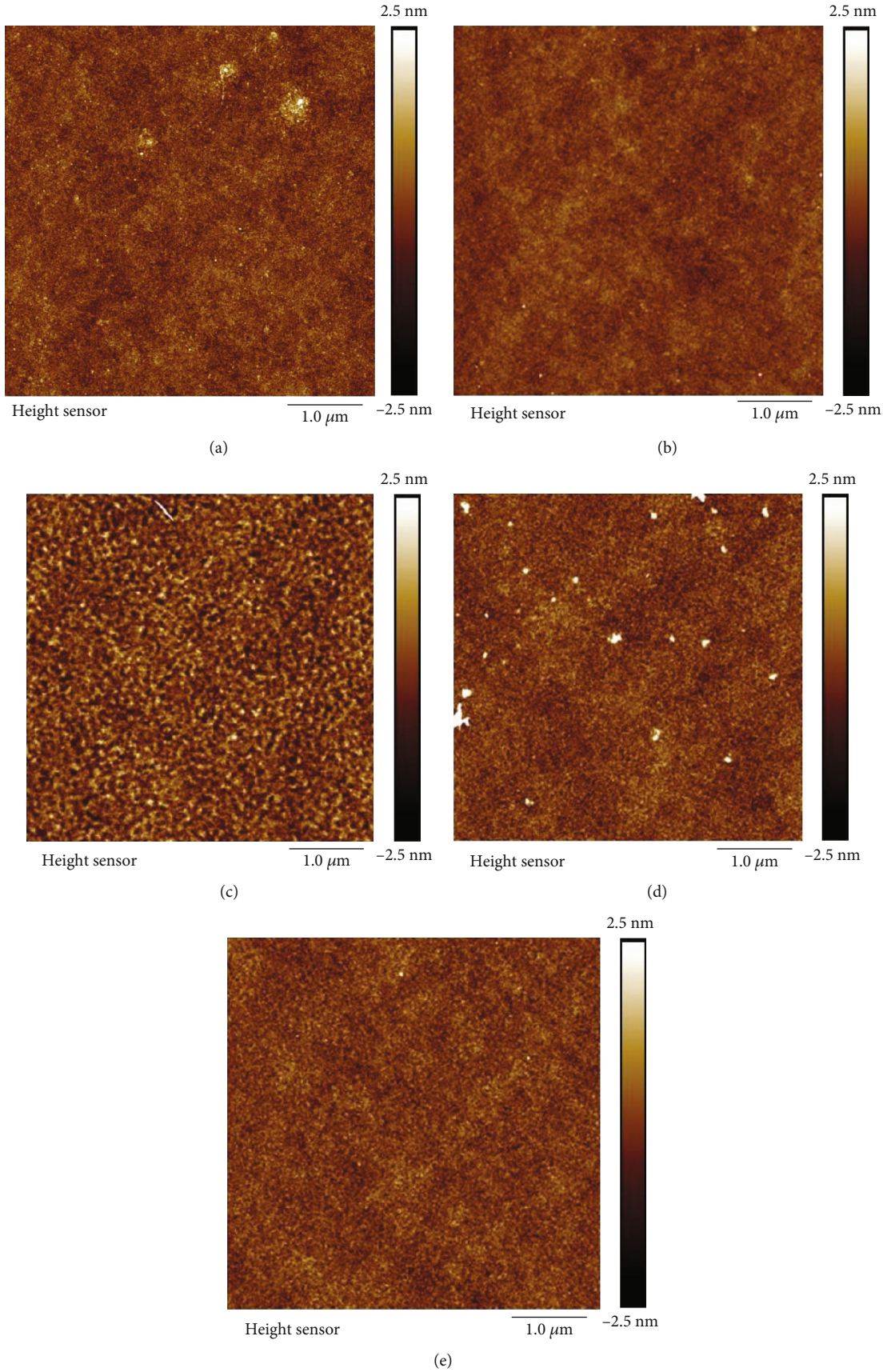

Figure 10: Surface roughness of $Co_{40}Fe_{40}W_{20}$ thin films with various thicknesses: (a) 18 nm, (b) 30 nm, (c) 42 nm, (d) 60 nm, and (e) 90 nm.

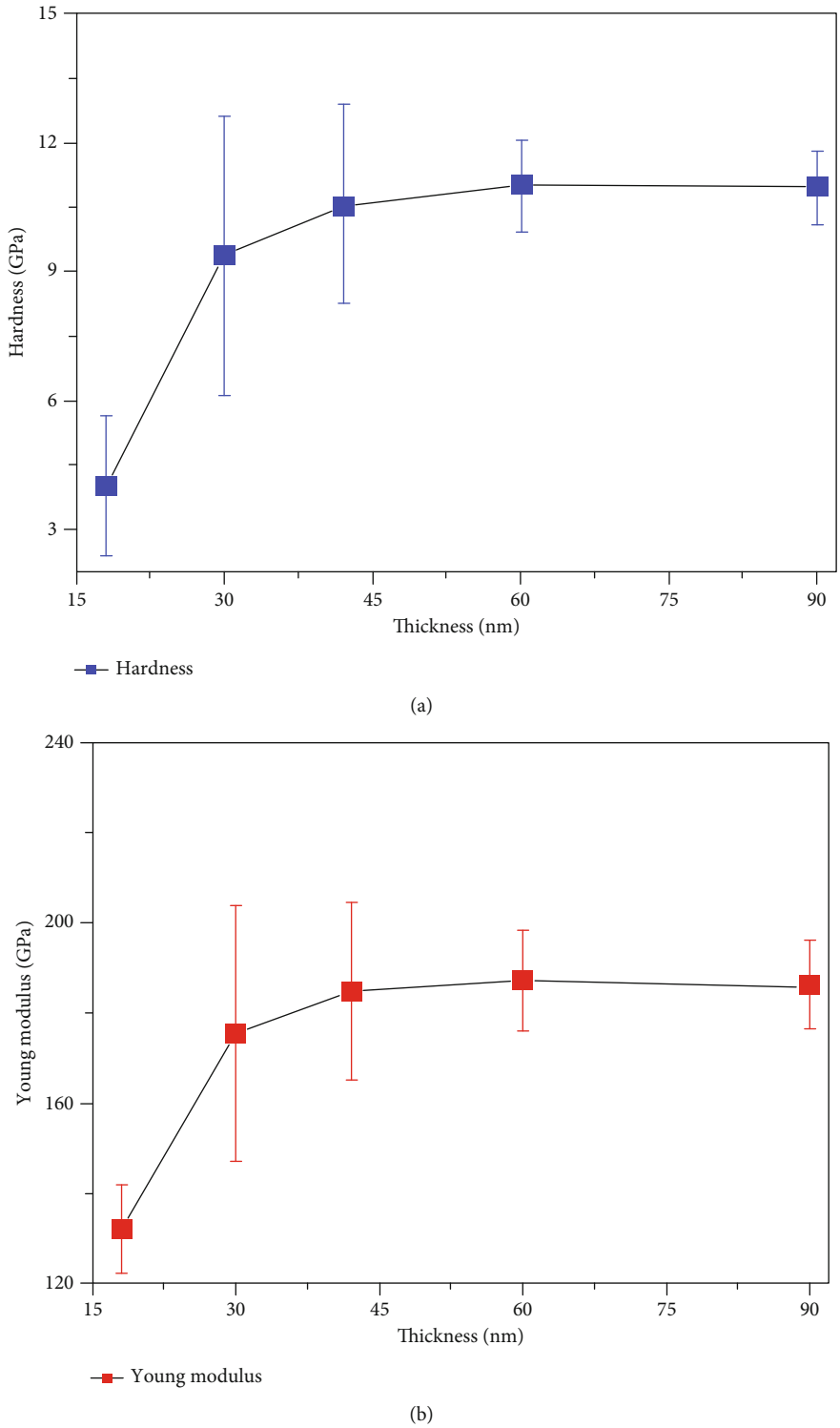

Figure 11: The analysis of nanoindentation of $Co_{40}Fe_{40}W_{20}$ thin films: (a) hardness and (b) Young's modulus.

the $Co_{40}Fe_{40}W_{20}$ films had soft magnetism. Furthermore, the contact angles of the $Co_{40}Fe_{40}W_{20}$ films were smaller than 90°, indicating that the films were hydrophilic. The surface energy had a downward concave feature, and the critical thickness was 42 nm. The high surface energy corresponded to strong adhesion. The increased surface roughness can induce domain wall pinning effect and high surface energy, causing a high coercivity and strong adhesion. Furthermore, the hardness and Young's modulus of CoFeW films are also displayed to saturated tendency when increasing thickness.

Data Availability

The data used to support the findings of this study are available from the corresponding author upon request.

Disclosure

The funders had no role in the design of the study; in the collection, analyses, or interpretation of data; in the writing of the manuscript; or in the decision to publish the results.

Conflicts of Interest

The authors declare that there is no conflict of interests regarding the publication of this paper.

Authors' Contributions

W.-J.L., S.-L.O., and Y.-T.C. are responsible for the conceptualization. Y.-T.C., Y.-C.L., C.-Y.C., and C.-C.C performed the methodology. Y.-H.C., Y.-C.L., and C.-Y.C. are involved in the validation and formal analysis. Y.-T.C. and W.-J.L. did the the investigation. T.-H.W. acquired the resources. Y.-T.C. is responsible for the original draft preparation. Y.-T.C. and W.-J.L. reviewed and edited the manuscript. Y.-T.C. and S.-L.O. supervised the study. Y.-T.C. and T.-H.W. are assigned to the project administration. W.-J.L. and Y.-H.C are involved in the funding acquisition. All authors have read and agreed to the published version of the manuscript.

Acknowledgments

This work was supported by the Ministry of Science and Technology (grant Nos. MOST108-2221-E-224-015-MY3 and MOST105-2112-M-224-001) and the National Yunlin University of Science and Technology (grant No. 109T01).

References

[1] E. P. George, A. N. Gubbi, I. Baker, and L. Robertson, "Mechanical properties of soft magnetic FeCo alloys," *Materials Science and Engineering A*, vol. 329, pp. 325–333, 2002.

[2] S. N. Kim, K. H. Chung, J. W. Choi, and S. H. Lim, "Manipulation of free-layer bias field in giant-magnetoresistance spin valve by controlling pinned-layer thickness," *Journal of Alloys and Compounds*, vol. 823, p. 153727, 2020.

[3] M. Zeng, B. J. Chen, and S. T. Lim, "Interfacial electric field and spin-orbitronic properties of heavy-metal/CoFe bilayers," *Applied Physics Letters*, vol. 114, no. 1, p. 012401, 2019.

[4] L. I. Naumova, M. A. Milyaev, R. S. Zavornitsyn, T. P. Krinitsina, V. V. Proglyado, and V. V. Ustinov, "Spin valve with a composite dysprosium-based pinned layer as a tool for determining Dy nanolayer helimagnetism," *Current Applied Physics*, vol. 19, no. 11, pp. 1252–1258, 2019.

[5] S. Noh, D. H. Kang, and M. Shin, "Simulation of strain-assisted switching in synthetic antiferromagnetic free layer-based magnetic tunnel junction," *IEEE Transactions on Magnetics*, vol. 55, no. 4, article 3400705, 2019.

[6] S. N. Kim, J. W. Choi, and S. H. Lim, "Tailoring of magnetic properties of giant magnetoresistance spin valves via insertion of ultrathin non-magnetic spacers between pinned and pinning layers," *Scientific Reports*, vol. 9, no. 1, p. 1617, 2019.

[7] C. Swindells, A. T. Hindmarch, A. J. Gallant, and D. Atkinson, "Spin current propagation through ultra-thin insulating layers in multilayered ferromagnetic systems," *Applied Physics Letters*, vol. 116, no. 4, p. 042403, 2020.

[8] S. L. Ou, W. J. Liu, Y. H. Chang et al., "Structure, magnetic property, surface morphology, and surface energy of $Co_{40}Fe_{40}V_{10}B_{10}$ films on Si(100) substrate," *Applied Sciences*, vol. 10, no. 2, p. 449, 2020.

[9] T. Ogasawara, M. Oogane, M. A. Mahdawi, M. Tsunoda, and Y. Ando, "Effect of second-order magnetic anisotropy on nonlinearity of conductance in CoFeB/MgO/CoFeB magnetic tunnel junction for magnetic sensor devices," *Scientific Reports*, vol. 9, no. 1, p. 17018, 2019.

[10] T. Devolder, S. Couet, J. Swerts, S. Mertens, S. Rao, and G. S. Kar, "Effect of tantalum spacer thickness and deposition conditions on the properties of MgO/CoFeB/Ta/CoFeB/MgO free layers," *IEEE Magnetics Letters*, vol. 10, p. 5505804, 2019.

[11] H. Honjo, S. Ikeda, H. Sato et al., "Impact of tungsten sputtering condition on magnetic and transport properties of double-MgO magnetic tunneling junction with CoFeB/W/CoFeB free layer," *IEEE Transactions on Magnetics*, vol. 53, no. 11, p. 2501604, 2017.

[12] O. Manos, P. Bougiatioti, D. Dyck et al., "Correlation of tunnel magnetoresistance with the magnetic properties in perpendicular CoFeB-based junctions with exchange bias," *Journal of Applied Physics*, vol. 125, no. 2, p. 023905, 2019.

[13] H. Lv, J. Fidalgo, A. V. Silva et al., "Assessment of conduction mechanisms through MgO ultrathin barriers in CoFeB/MgO/-CoFeB perpendicular magnetic tunnel junctions," *Applied Physics Letters*, vol. 114, no. 10, p. 102402, 2019.

[14] J. M. I. Harms, G. Jan, S. S. Guisan et al., "Ultrathin perpendicular magnetic anisotropy CoFeB free layers for highly efficient, high speed writing in spin-transfer-torque magnetic random access memory," *Scientific Reports*, vol. 9, no. 1, p. 19407, 2019.

[15] C. F. Pai, L. Liu, Y. Li, H. W. Tseng, D. C. Ralph, and R. A. Buhrman, "Spin transfer torque devices utilizing the giant spin Hall effect of tungsten," *Applied Physics Letters*, vol. 101, no. 12, p. 122404, 2012.

[16] Z. Ghaferi, S. Sharafi, and M. E. Bahrololoomb, "The role of electrolyte pH on phase evolution and magnetic properties of CoFeW codeposited films," *Applied Surface Science*, vol. 375, pp. 35–41, 2016.

[17] J. Sun, H. Li, Y. Huang, and Z. Zhuang, "CoFeW ternary oxides nanoparticles for oxygen evolution reaction," *Materials Letters*, vol. 223, pp. 246–249, 2018.

[18] S. Mehrizi, M. Heydarzadeh Sohi, and S. A. Seyyed Ebrahimi, "Study of microstructure and magnetic properties of electrodeposited nanocrystalline CoFeNiCu thin films," *Surface and Coating Technology*, vol. 205, no. 20, pp. 4757–4763, 2011.

[19] L. Ricq, F. Lallemand, M. P. Gigandet, and J. Pagetti, "Influence of sodium saccharin on the electrodeposition and characterization of CoFe magnetic film," *Surface and Coating Technology*, vol. 138, no. 2-3, pp. 278–283, 2001.

[20] E. E. Kalu, R. Bell, and M. Dupree, "Improvement of the corrosion behavior of electrodeposited CoFeCu thin films," *Materials Chemistry and Physics*, vol. 124, no. 1, pp. 689–693, 2010.

[21] T. P. Kumari, M. M. Raja, A. Kumar, S. Srinath, and S. V. Kamat, "Effect of thickness on structure, microstructure, residual stress and soft magnetic properties of DC sputtered

$Fe_{65}Co_{35}$ soft magnetic thin films," *Journal of Magnetism and Magnetic Materials*, vol. 365, pp. 93–99, 2014.

[22] H. Kockar, E. Ozergin, O. Karaagac, and M. Alper, "Characterisations of CoFeCu films: influence of Fe concentration," *Journal of Alloys and Compounds*, vol. 586, pp. 326–330, 2014.

[23] K. Ma, T. S. Chung, and R. J. Good, "Surface energy of thermotropic liquid crystalline polyesters and polyesteramide," *Journal of Polymer Science*, vol. 36, no. 13, pp. 2327–2337, 1998.

[24] D. K. Owens and R. C. Wendt, "Estimation of the surface free energy of polymers," *Journal of Applied Polymer Science*, vol. 13, no. 8, pp. 1741–1747, 1969.

[25] D. H. Kaelble and K. C. Uy, "A reinterpretation of organic liquid-polytetrafluoroethylene surface interactions," *The Journal of Adhesion*, vol. 2, no. 1, pp. 50–60, 2008.

[26] S. Maruyama, T. Kurashige, S. Matsumoto, Y. Yamaguchi, and T. Kimura, "Liquid droplet in contact with a solid surface," *Microscale Thermophysical Engineering*, vol. 2, no. 1, pp. 49–62, 1998.

[27] W. J. Liu, Y. T. Chen, Y. H. Chang et al., "Structure and magnetic properties of Co40Fe40V20Thin films," *Journal of Nanoscience and Nanotechnology*, vol. 19, no. 9, pp. 5974–5978, 2019.

[28] H. Kakati, A. R. Pal, H. Bailung, and J. Chutia, "Deposition of nanostructured crystalline and corrosion resistant alumina film on bell metal at low temperature by rf magnetron sputtering," *Applied Surface Science*, vol. 255, no. 16, pp. 7403–7407, 2009.

[29] G. Choe and M. Steinback, "Surface roughness effects on magnetoresistive and magnetic properties of NiFe thin films," *Journal of Applied Physics*, vol. 85, no. 8, pp. 5777–5779, 1999.

[30] G. Bhatia, A. Srivastava, and P. C. Srivastava, "Effect of ion irradiation on magnetic property of exchange coupled interfacial structures of Fe/NiO and NiO/Fe on Si substrates," *Radiation Effects and Defects in Solids*, vol. 169, no. 6, pp. 529–537, 2014.

[31] A. M. P. Sakita, E. C. Passamani, H. Kumar et al., "Influence of current density on crystalline structure and magnetic properties of electrodeposited Co-rich CoNiW alloys," *Materials Chemistry and Physics*, vol. 141, no. 1, pp. 576–581, 2013.

[32] R. D. Noce, A. V. Benedetti, M. Magnani et al., "Structural, morphological and magnetic characterization of electrodeposited Co–Fe–W alloys," *Journal of Alloys and Compounds*, vol. 611, no. 20, pp. 243–248, 2014.

[33] B. D. Cullity, *Elements of X-Ray Diffraction*, Addison-Wesley, Reading, MA, 2nd edition, 1978.

[34] D. Xue, G. Chai, X. Li, and X. Fan, "Effects of grain size distribution on coercivity and permeability of ferromagnets," *Journal of Magnetism and Magnetic Materials*, vol. 320, no. 8, pp. 1541–1548, 2008.

[35] M. Khajepour and S. Sharafi, "Structural and magnetic properties of nanostructured $Fe_{50}(Co_{50})$-6.5 wt% Si powder prepared by high energy ball milling," *Journal of Alloys and Compounds*, vol. 509, no. 29, pp. 7729–7737, 2011.

[36] S. Y. Yang, J. J. Chien, W. C. Wang et al., "Magnetic nanoparticles for high-sensitivity detection on nucleic acids via superconducting-quantum-interference-device-based immunomagnetic reduction assay," *Journal of Magnetism and Magnetic Materials*, vol. 323, no. 6, pp. 681–685, 2011.

[37] Y. T. Chen, S. M. Xie, and H. Y. Jheng, "The low-frequency alternative-current magnetic susceptibility and electrical properties of Si(100)/$Fe_{40}Pd_{40}B_{20}$(X Å)/ZnO(500 Å) and Si(100)/ZnO(500 Å)/$Fe_{40}Pd_{40}B_{20}$(Y Å) systems," *Journal of Applied Physics*, vol. 113, no. 17, p. 17B303, 2013.

[38] S. H. Kong, T. Okamoto, and S. Nakagawa, "[Ni-Fe/Si] double seedlayer with low surface energy for Fe-Co-B soft magnetic underlayer with High<tex>$H_rm k$</tex>for perpendicular magnetic recording media," *IEEE Transactions on Magnetics*, vol. 40, no. 4, pp. 2389–2391, 2004.

[39] D. A. Porter and K. E. Easterling, *Phase transformations in metals and alloy*, CRC Press, London, 2nd edition, 1992.

[40] J. Swerts, K. Temst, N. Vandamme, C. Van Haesendonck, and Y. Bruynseraede, "Interplay between surface roughness and magnetic properties in Ag/Fe bilayers," *Journal of Magnetism and Magnetic Materials*, vol. 240, no. 1–3, pp. 380–382, 2002.

[41] Y. P. Zhao, R. M. Gamache, G. C. Wang, T. M. Lu, G. Palasantzas, and T. M. D. Hosson, "Effect of surface roughness on magnetic domain wall thickness, domain size, and coercivity," *Journal of Applied Physics*, vol. 89, no. 2, pp. 1325–1330, 2001.

[42] M. Zou, S. Beckford, R. Wei, C. Ellis, G. Hatton, and M. A. Miller, "Effects of surface roughness and energy on ice adhesion strength," *Applied Surface Science*, vol. 257, no. 8, pp. 3786–3792, 2011.

[43] W. Deng and H. Kesari, "Depth-dependent hysteresis in adhesive elastic contacts at large surface roughness," *Scientific Reports*, vol. 9, no. 1639, pp. 1–12, 2019.

[44] W. C. Oliver and G. M. Pharr, "An improved technique for determining hardness and elastic modulus using load and displacement sensing indentation experiments," *Journal of Materials Research*, vol. 7, no. 6, pp. 1564–1583, 1992.

[45] J. Zhu, J. Han, A. Liu, S. Meng, and C. Jiang, "Mechanical properties and Raman characterization of amorphous diamond films as a function of film thickness," *Surface and Coating Technology*, vol. 201, no. 15, pp. 6667–6669, 2007.